



Letter

Autophagy restricts tomato fruit ripening via a general role in ethylene repression

Introduction

Ripening involves complex biochemical and molecular reprogramming, resulting in color, texture, aroma, and flavor changes to attract humans and other animals (Giovannoni *et al.*, 2017). In climacteric fruits, this process is controlled by a myriad of phytohormones, predominantly ethylene (Li *et al.*, 2021; Huang *et al.*, 2022). To allow these changes, fruits constantly reshape their cellular proteome by fine-tuning protein degradation and synthesis (Szymanski *et al.*, 2017). While the ubiquitin–proteasome system was shown to be critical in ethylene signaling and ripening (Fenn & Giovannoni, 2021; Jia *et al.*, 2023), knowledge of the impact of autophagy, another central degradation system, is rather limited.

Autophagy delivers cytosolic components to the vacuole for degradation and recycling. Double-membrane vesicles, termed autophagosomes, are generated around the cellular cargo destined for degradation. The autophagosome then fuses with the tonoplast to release a single membrane structure, termed autophagic body. Inside of the vacuole, the autophagic body degrades along with its cargo, and its constituents are recycled to replenish cellular energy. Autophagy is executed via the function of > 30 autophagy-related (ATG) proteins (Ding *et al.*, 2018; Marshall & Vierstra, 2018). Notably, ATG proteins annotated with different numbers are not related and have distinct roles in autophagy. Among these, the ubiquitin-like ATG8 proteins are important for autophagosome biogenesis, fusion with the vacuole, and selective recognition of the cargo to be degraded. They are found conjugated either to phosphatidylethanolamine (PE) lipids (lipidated) or in a nonactive (nonlipidated) free form (Kellner *et al.*, 2017). The ATG8 family consists of nine members in *Arabidopsis thaliana* (*Arabidopsis*; AtATG8a to AtATG8i). When conjugated to a fluorescent protein, ATG8 family proteins are considered optimal markers for autophagy activity (or flux) assessment, as the stability of the fluorescent protein moiety allows for the estimation of the amount of autophagic material that was delivered to the vacuole. While assessing the ATG8 lipidation status (ATG8-PE : ATG8 ratio) provides a measure of autophagic membrane levels in the cytosol, it does not necessarily reflect autophagy activity (Qi *et al.*, 2023). Due to some level of redundancy (Del Chiaro *et al.*, 2024), ATG8 family members are not used for functional analysis. Alternatively, the downregulation of other essential (and usually single-copy) ATG genes, such as *ATG2*, *ATG5*, or *ATG7*, each independently, can serve for functional analysis (Marshall & Vierstra, 2018). Each of

these genes has a critical role in autophagy, rendering the respective knockout mutant autophagy-deficient. ATG2, together with ATG9 and ATG18 family proteins, functions in the lipid delivery system to the developing phagophore. Recently, the ATG2-dependent recruitment of ATG18a onto the phagophore to promote its expansion and closure was revealed (Luo *et al.*, 2023). ATG5 and ATG7 are responsible for different yet essential steps of the ubiquitin-like conjugation of ATG8 proteins to autophagic membranes. *ATG4*, a protease allowing the lipidation or delipidation of ATG8 members, is represented by a single gene in *Solanum lycopersicum* (tomato) and two genes in *Arabidopsis* (*AtATG4a* and *AtATG4b*) and is also used for functional analysis (Seo *et al.*, 2016).

Initially, it was assumed that ethylene and autophagy are not linked based on the lack of leaf senescence recovery phenotype in *Arabidopsis* plants deficient in autophagy and *Ethylene-Insensitive 2* genes (Yoshimoto *et al.*, 2009). However, several studies later suggested that such an interaction exists (Liao *et al.*, 2022). First, the transcript abundance of several ethylene biosynthesis and ethylene signaling genes was higher in *atg5* and *atg9* mutants than in wild-type (WT) (*Col-0*) *Arabidopsis* plants (Masclaux-Daubresse *et al.*, 2014). Moreover, tomato plants treated with the ethylene precursor, 1-aminocyclopropane-1-carboxylate (ACC), exhibited increased autophagy activity and expression of *SLATG8d* and *SLATG18b* genes during drought. The authors suggested the direct binding of Ethylene Response Factor 5 to the promoters of these genes (Zhu *et al.*, 2018). 1-Aminocyclopropane-1-carboxylate was also reported to induce autophagy in *Arabidopsis* (Rodriguez *et al.*, 2020). Finally, pollination-induced petal leaf senescence, accompanied by enhanced ethylene emission, was further accompanied by increased expression of petunia PhATG8 isoforms and generation of autophagosomes. Notably, the ethylene antagonist, 1-methylcyclopropene (1-MCP), delayed the induction of PhATG8 proteins following pollination and the appearance of the subcellular structures presumed to be autophagosomes (Shibuya *et al.*, 2013). Therefore, ethylene is repeatedly suggested to regulate autophagy. Nonetheless, it is yet unclear whether autophagy has any regulatory impact on ethylene and whether it is involved in climacteric fruit ripening.

Materials and Methods

Plant growth and transformation

Tomato (*Solanum lycopersicum* L.) Micro-Tom, Moneymaker and Ailsa Craig cultivars, and *Arabidopsis thaliana* (L.) Heynh. Col-0 ecotype were used in this study. Tomatoes were grown in pots at 23°C in a climate-controlled glasshouse under a 12-h, light : dark cycle. *Arabidopsis* was grown in growth chambers at 16 h : 8 h, 22°C, light : dark cycles. Transgenic Del/Ros1 Micro-Tom (Orzaez *et al.*, 2009) seeds were obtained from Prof. Asaph Aharoni's laboratory (Weizmann Institute). GFP-SLATG8-2.2 Moneymaker

lines were generated by transforming the 35S::GFP-StATG8-2.2 construct (Potato StATG8-2.2 is identical to the tomato counterpart), which was kindly provided by Dr Yasin Dagdas (Zess *et al.*, 2019). E8::SLATG4-RNAi lines were generated in a Micro-Tom background.

Tomato transformation with the E8::ATG4-RNAi construct was performed using *Agrobacterium* strain GV3101 harboring the appropriate plasmids as described in Sun *et al.* (2015) with minor modifications. Tomato seeds were surface-sterilized and germinated on a ½-strength Murashige & Skoog (MS) medium (+30 g l⁻¹ sucrose). After 10 d, fully expanded cotyledons were dissected, with only their central sections used. Explants were immersed in *Agrobacterium* suspensions (OD₆₀₀ = 0.6) for 20 min. Explants were then gently dried on Whatman paper and transferred to a cocultivation medium (MS medium supplemented with 3% (w/v) sucrose, 0.8% agar, and 2 mg l⁻¹ 6-Benzylaminopurine) for 2 d in the dark. Then, explants were transitioned to a shoot induction medium (MS medium supplemented with 1 mg l⁻¹ zeatin, along with 0.8% (w/v) agar, 3% (w/v) sucrose, 50 mg l⁻¹ kanamycin, and 500 mg l⁻¹ cefotaxime). Incubation took place at 26°C with a 16-h photoperiod. After 30 d, plantlets were separated from the original explants and transferred to a fresh induction medium. Shoots reaching lengths of 2–3 cm were excised and transplanted to a root induction medium (MS medium containing 1 mg l⁻¹ indole-3-acetic acid (IAA), 0.3% (w/v) agar, 3% (w/v) sucrose, and 50 mg l⁻¹ kanamycin). All substances used were from Duchefa Biochemie (Haarlem, the Netherlands). Eventually, 20 lines were obtained, of which five lines (L2, L9, L15, L18, and L20) were examined postharvest, all showing a clear delayed ripening phenotype at their T2 generation. Progeny of some lines, such as L9 (T3 and T4 generations), showed a reduction in phenotype severity, potentially due to *trans*-generational silencing of the transgene.

GFP-SLATG8-2.2 Moneymaker line was generated similarly with a few differences. The seeds were sown on a germination medium (4.3 g l⁻¹ MS including vitamins, 30 g l⁻¹ sucrose, 100 mg l⁻¹ myo-inositol, 0.8% phytoagar, pH 5.8). Two microliters of the *Agrobacterium* suspension (10 mM MgSO₄, 200 µM acetosyringone; OD₆₀₀ = 1.0) was applied per cotyledon, and they were cocultivated on the germination medium supplemented with 1 mg l⁻¹ 6-Benzylaminopurine and 1 mg l⁻¹ NAA for 2 d in the dark at 22°C. In 2 d, the cotyledons were placed abaxial surface down on the germination medium supplemented with 35 mg l⁻¹ kanamycin, 1 mg l⁻¹ *trans*-Zeatin, and 250 mg l⁻¹ ticarcillin disodium/clavulanate potassium. The cotyledons were placed in 14 h : 10 h, 23°C, light : dark, 50% humidity, and were transferred to a fresh selection medium every 7 d. In the second and fourth weeks, kanamycin concentration was increased to 50 and 100 mg l⁻¹, respectively. Regenerating shoots were cut at the base and transferred to the germination medium supplemented with 20 mg l⁻¹ kanamycin, 0.1 mg l⁻¹ IAA, and vancomycin (500 mg l⁻¹).

Plasmid construction

We employed the ClonExpress II One Step Cloning (Vazyme Biotech, Jiangsu, China) and the Gateway Cloning system (Thermo Fisher Scientific, Waltham, MA, USA) for virus-induced gene silencing

(VIGS)-related cloning. The 'VIGS tool' at the Sol Genomics Network website (vigs.solgenomics.net) was used to select appropriate 300 base-pair sequences. The primers used are listed in Supporting Information Table S1. Approximately 300-bp fragments of SLATG2 (Soly01g108160) and SLATG7 (Soly01g068930) were PCR-amplified and cloned into pENTER-Gus (Thermo Fisher Scientific; modified to have spectinomycin instead of kanamycin resistance). Then, the Gateway LR reaction was performed to allow the transfer of the gene fragment into the pTRV2-Del/Ros1 vector. For ripening-specific SLATG4 (Soly01g006230) silencing, the E8::SLATG4-RNAi vector was generated by switching the promoter in the 35S::SLATG4-RNAi expression cassette (Alseekh *et al.*, 2022). The original plasmid was amplified (Phusion polymerase) as a linear fragment without the 35S part. Then, ClonExpress II was employed to introduce a PCR-amplified E8 promoter with compatible flanking regions of the linearized plasmid. All cloned plasmids were transformed into the Mix & Go DH5α competent cells (Zymo Research, Irvine, CA, USA) and selected on Luria Broth (LB) agar plates containing the relevant antibiotics. Colony PCR confirmed positive clones, and plasmids were then purified using the Promega plasmid purification kit.

Immunoblotting

Liquid nitrogen-frozen tomato fruit pericarp samples were manually ground to a fine powder using a mortar and pestle. One gram of samples was mixed with 500 µl of a 1× Laemmli buffer. The mixture was then heated to 95°C for 5 min and centrifuged at 16 000 g (4°C) for 10 min. The resulting supernatant was collected for immunoblotting. To allow the separation of ATG8 and ATG8-PE fragments, equal amounts of protein were loaded onto custom-made 15% SDS-PAGE gels supplemented with 6 M urea in the resolving gel. Gels were blotted onto polyvinylidene difluoride membranes, which were incubated overnight at 4°C with 1 : 1000 anti-ATG8 antibodies (Abcam, Cambridge, UK) and subsequently with goat-anti-rabbit-HRP (1 : 10 000; Jackson ImmunoResearch, West Grove, PA, USA) before visualization in the Fusion Plus Imaging System (Vilber, Marne-la-Vallée, France). Anti-H3 antibodies (EMD Millipore Corp., Burlington, MA, USA) were used for loading visualization (1 : 10 000). For the GFP-release assay, total protein extracts were loaded onto commercial precast gels (SurePage; GenScript, Piscataway, NJ, USA) and immunoblotted with anti-GFP antibodies (Ab290; 1 : 2000; Abcam). *Arabidopsis* samples were processed as previously described (Michaeli *et al.*, 2019).

RNA isolation and qRT-PCR

Total RNA was extracted from 100 mg of young leaves (three biological replicates) or pink-stage tomato fruits (three biological replicates, each comprised of three pooled fruits) using the Plant Spectrum RNA isolation kit (Sigma). RNA concentration and purity were determined, and cDNA was synthesized from 1 µg of total RNA using the verso cDNA synthesis kit (Thermo Fisher Scientific). For quantitative polymerase chain reaction (qPCR), the cDNA of each sample was diluted 1 : 10 with nuclease-free water before mixing with the Luna® Universal qRT-PCR Master Mix

(New England Biolabs, Ipswich, MA, USA). Then, samples were processed using the StepOnePlus Real-Time PCR System (Thermo Fisher Scientific). The comparative C_t ($\Delta\Delta C_t$) method was employed for data analysis, normalizing target gene expression to reference genes (TIP41, GAPDH, and Actin) and comparing the relative expression levels between samples.

Virus-induced gene silencing

pTRV1 and pTRV2-Del/Ros1 harboring the SIATG7- or SIATG2-derived fragments were introduced into *Agrobacterium* strain GV3101 using electroporation (Bio-Rad). A 5-ml culture was grown overnight at 28°C in a medium containing kanamycin. The next day, the culture was transferred to a 50-ml LB medium containing antibiotics, 10 mM 2-(N-morpholino)ethanesulfonic acid (MES), and 20 μ M acetosyringone and grown overnight in a 28°C shaker. *Agrobacterium* cells were harvested, resuspended in an infiltration medium (10 mM $MgCl_2$, 10 mM MES, and 200 μ M acetosyringone), left at room temperature for 3 h, and adjusted to an optical density (OD_{600}) of 0.1. *Agrobacterium* cells were then infiltrated, using a 1-ml syringe, through the peduncle of mature-green (MG)-stage fruits while attached to the plant.

Fluorescence imaging and quantification of transgenic fruits using the *in vivo* imaging system

GFP-SIATG8-2.2 tomato fruits were harvested at different ripening stages (MG, turning, and red-ripe (RR)) and kept in the dark for 12 h before evaluation. GFP fluorescence (465 nm excitation and 520 nm detection) was acquired and analyzed using the *in vivo* imaging system (IVIS) Lumina II equipped with an XFOV-24 lens and the LIVING IMAGE 4.3.1 software (PerkinElmer, Waltham, MA, USA). Fluorescence is presented as radiance intensity (photons $s^{-1} cm^{-2} sr^{-1}$).

Confocal microscopy, ConA treatment, and quantification

Confocal imaging was performed using the Leica SP8 (Leica Microsystems, Wetzlar, Germany) confocal laser-scanning microscopy (CLSM) system at the Volcani Institute microscopy core facility. Thin sections of tomato fruit pericarp (using razor blades) or intact *Arabidopsis* seedlings were positioned between a microscope slide and a coverslip containing a $\frac{1}{2}$ MS liquid medium. Excitation/detection-range parameters for GFP were 488 nm/500–550 nm, and emissions were collected using the system's hybrid (Hyd) detectors. $\times 20$ dry (NA 0.75) or $\times 63$ water immersion (NA 1.3) objectives were used. Scanning was routinely performed in 'line' mode. The images were processed and analyzed using Fiji (IMAGEJ).

For concanamycin A (ConA) treatment of fruit cells, thin fruit sections were incubated in liquid $\frac{1}{2}$ MS supplemented with 2 or 10 μ M ConA, or the corresponding amount of dimethyl sulfoxide (DMSO) (mock), for 7 h before imaging or 15 h for immunoblots. For *Arabidopsis* analysis, GFP-ATG8E seeds were germinated in liquid $\frac{1}{2}$ MS (Duchefa Biochemie) medium containing 1% sucrose. Four-day-old seedlings were transferred into the same medium containing either 0.4% DMSO (Sigma-Aldrich; as mock) or 20 μ M

ACC or 1 μ M ConA (Santa Cruz Biotechnology, Dallas, TX, USA) and 0.4% DMSO or 1 μ M ConA and 20 μ M ACC. Seedlings were incubated for 2 h in the dark and transferred to slides in the corresponding medium. Labeled autophagosomes were counted manually from single confocal-slice images. Forty-five seedlings and 677 cells were analyzed in three independent experiments.

Triple-response assay

The triple-response assay was made as described previously (Merchante & Stepanova, 2017) with minor modifications. Sterilized seeds were placed onto plates containing a $\frac{1}{2}$ MS medium (Duchefa Biochemie) and 1% sucrose, with or without 20 μ M ACC. The plates were then moved to 4°C in darkness for 48 h before exposure to light for 2 h. Then, the plates were relocated to the growth room (22°C) and kept in darkness for 72 h.

Phylogenetic tree construction

The amino-acid sequences of tomato and *Arabidopsis* ATG8 proteins were retrieved from Sol Genomics Network (solgenomics.net) and TAIR (www.arabidopsis.org) databases. Sequences were aligned using CLUSTALW in the EMBL-EBI web server (<https://www.ebi.ac.uk/Tools/msa/clustalw2/>) using the default settings. The resulting file was uploaded to IQ-TREE v.1.6 (<http://www.iqtree.org/>) for phylogenetic analysis, which included MODELFINDER, tree reconstruction, and ultrafast bootstrap with 1000 replicates. MODELFINDER was used to determine the best-fit model, with the Bayesian information criterion guiding the model selection, ultimately choosing LG + G4. This model, incorporating a gamma distribution with four rate categories, was used for managing rate heterogeneity among sites. Branch support values were calculated using the SH-aLRT test and ultrafast bootstrap approximation with 1000 replicates. Finally, the tree was visualized in the Newick format, using the Interactive Tree of Life (iTOL) web-based tool (<https://itol.embl.de/>). The tree image was exported and refined using INKSCAPE to enhance clarity and presentation.

Fruit color (hue) and firmness measurements

Color values a^* and b^* and the hue parameter were measured using the Konica Minolta Chroma Meter CR-400 Series v.1.11 (Konica Minolta, Tokyo, Japan). Fruits were considered at the MG stage when $-0.59 < a^*/b^* < -0.47$ (Batu, 2004). Then, fruits were harvested, cleaned, and measured for hue and firmness on different days postharvest, as indicated in related figures. Firmness was measured using the TA.XT Plus Texture Analyzer (Stable Microsystems, Surrey, UK) using a 3-mm-diameter probe with 5% penetration at a speed of 1 mm s^{-1} , recording the maximal endpoint force in Newtons (N).

Ethylene production measurements and 1-MCP treatment

Harvested fruits were placed in 200-ml sealed containers for 2 h. Ethylene was measured by injecting 10 ml of head-space air into a gas chromatograph (GC; Varian 3300, Walnut Creek, CA, USA) with a flame ionization detector and an alumina column. For

Arabidopsis, seedlings of the different genotypes were grown on a $\frac{1}{2}$ MS + 1% sucrose solid medium. 1-Aminocyclopropane-1-carboxylate and mock treatments were applied on 10-d-old seedlings by adding 20 μ M ACC (dissolved in a liquid $\frac{1}{2}$ MS medium) or mock (a ACC-free $\frac{1}{2}$ MS medium) to the plates. Following 96 h of incubation, seedlings were removed, weighed, and quickly sealed in 20-ml syringes containing a 1-ml $\frac{1}{2}$ MS liquid medium, with or without ACC, for 2 h. Each syringe contained 30 seedlings. Head-space was then collected with a fresh 10-ml syringe (by penetrating the needle into the 20-ml syringe) and injected into the GC apparatus. For 1-MCP treatment, fruits from WT and the E8::ATG4-RNAi lines were placed in a sealed flask containing 600 ppb of 1-MCP (RIMI, Petah Tikva, Israel) for 20 h. Then, fruits were released and placed in a 'shelf-life' chamber (22°C) for the indicated duration for hue measurements.

Dark-induced leaf senescence and electrolyte leakage measurements

The third leaf from the apical meristem of 5-wk-old E8::ATG4-RNAi lines (L9, L15, and L18) and WT plants was detached. Leaves were then washed and kept in Petri dishes with moist Whatman paper. Petri dishes were then wrapped with aluminum foil, incubated in a growth chamber, and photographed at 5, 7, 9, 12, and 14 d. Each experiment included four replicates. Similar leaves were used for electrolyte leakage measurements. From each leaf, 1.2-cm-diameter leaf disks were incubated in 10 ml of de-ionized water in the dark with solution measurements taken at 0, 3, 6, 7, 10, 11, 13, 17, 19, and 21 d using a conductivity meter. The experiment was repeated four times.

Statistics

Statistical analysis and data visualization were conducted using PYTHON 3.9.6 with the following libraries:

- (1) NumPy 1.25.2 for numerical operations and data handling;
- (2) Pandas 2.0.3 for data importation and data frame handling;
- (3) Matplotlib 3.7.2 for basic plotting; and
- (4) Seaborn 0.12.2 for advanced data visualization.

Calculations were performed using the subpackage SCIPY.STATS from the open-source SCIPY PYTHON-based library. The *Shapiro-Wilk* test (SCIPY.STATS.SHAPIRO – SCIPY v.1.11.2) was used for normality determination, where P -value > 0.05 suggests that the data are normally distributed. The *Levene's* test (SCIPY.STATS.LEVENE) was used for equal variance determination, where P -value > 0.05 suggests equal variance. If two datasets showed equal variance and normal distribution, then an independent two-sample t -test (SCIPY.STATS.TTEST_IND) was used. Otherwise, a nonparametric *Mann-Whitney U* test (SCIPY.STATS.MANNWHITNEYU) was used.

Results

Autophagy activity climaxes at mid-ripening

To decipher the role of autophagy in tomato fruit ripening, we first followed its activity by monitoring SLATG8 dynamics (Qi

et al., 2023). There are seven tomato protein orthologs of *Arabidopsis* AtATG8s clustered into four subgroups (Fig. 1a; Kellner *et al.*, 2017; Zess *et al.*, 2019). Data from the Sol Genomics Network – Tomato Expression Atlas (SGN-TEA; tea.solgenomics.net; Shinozaki *et al.*, 2018) revealed that five of the seven members showed increasing expression along ripening progression. Two of these, *SLATG8-1.1* (Solyc08g078820) and *SLATG8-2.2* (Solyc07g064680), exhibited a relatively higher transcript abundance (Fig. 1b). To verify that *SLATG8-2.2*, as a representative, encodes an autophagy-associated protein in fruit cells, we generated transgenic tomato plants expressing GFP-SLATG8-2.2. CLSM of fruit endocarp cells at the breaker stage highlighted small spherical bodies (1–2 μ m in diameter) reminiscent of autophagosomes (Fig. 1c, images C1–C3). These structures were motile (Video S1) and occasionally seemed to be ring-like structures. Shown here is a presumably mature phagophore at an advanced stage before closure (Fig. 1c, image C4, edges defined by arrowheads), later appearing as a fully closed and complete autophagosome (Fig. 1c, image C5).

To gain insight into autophagy activity, we immunoblotted total pericarp protein extracts of tomato fruits at different ripening stages with an anti-ATG8 antibody. We suspect this polyclonal antibody recognizes all expressed ATG8 isoforms. Our analysis showed a sharp increase in ATG8-PE levels, from undetectable levels at the MG stage to prominent expression at mid-ripening, and maintaining these high levels until the final RR stage (Fig. 1d). The increase in ATG8-PE may reflect either an elevation in autophagy activity or a blockage in autophagy flux to the vacuole. To determine which of these options is factual, GFP-SLATG8-2.2 expressing fruits were evaluated to follow autophagy flux. Using an IVIS (Perkin Elmer), we detected sufficient GFP fluorescence in fruits of MG to orange stages. However, the signal was not detected in any of the RR fruits examined ($n = 22$; Fig. 1e). We then employed the GFP-release assay, which allows assessment of autophagy flux from the cytoplasm to the vacuole according to the ratio of the free GFP degradation product relative to the full-length GFP-ATG8 fusion protein. Immunoblotting fruit protein extracts of three ripening stages, MG, orange, and RR, with anti-GFP antibodies revealed a sharp increase in free GFP level (i.e. increasing flux) from the MG stage to the orange stage (Fig. 1f). Consistent with our IVIS analysis (Fig. 1e), the level of GFP detection at the RR stage was significantly lower than at earlier stages. Nonetheless, it was sufficient to observe a shift back toward balanced levels of GFP-ATG8-2.2 and the free GFP, indicating a reduction in autophagy flux (Fig. 1f; RR sample). We then examined the impact of ConA, a drug that inhibits vacuolar degradation (Qi *et al.*, 2023). When applied at the orange stage, both mild (2 μ M) and high (10 μ M) ConA concentrations reduced the level of the free GFP degradation product (Fig. 1f, right blot), suggesting that most of it was produced via vacuolar degradation. ConA further allows visualization of fluorescent proteins within the vacuole lumen. CLSM imaging of orange-stage vacuoles following ConA treatment showed punctate structures corresponding to autophagic bodies (Fig. 1g), exhibiting the typical random movement within the vacuole lumen (Video S2). Notably, no such

autophagic bodies were detected in any of the MG-stage vacuoles following analysis of > 50 cells in 10 different fruits (Fig. 1g). This suggests autophagy flux occurs at the mid-ripening, whereas it is blocked at the MG stage. Altogether, increasing ATG8-PE levels along ripening renders increased autophagy activity, which peaks at the mid (orange) stage.

Autophagy deficiency accelerates fruit ripening and results in increased ethylene production in both tomato fruits and *Arabidopsis* seedlings

Autophagy is involved in many processes, including energy homeostasis and nutrient remobilization (Avin-Wittenberg

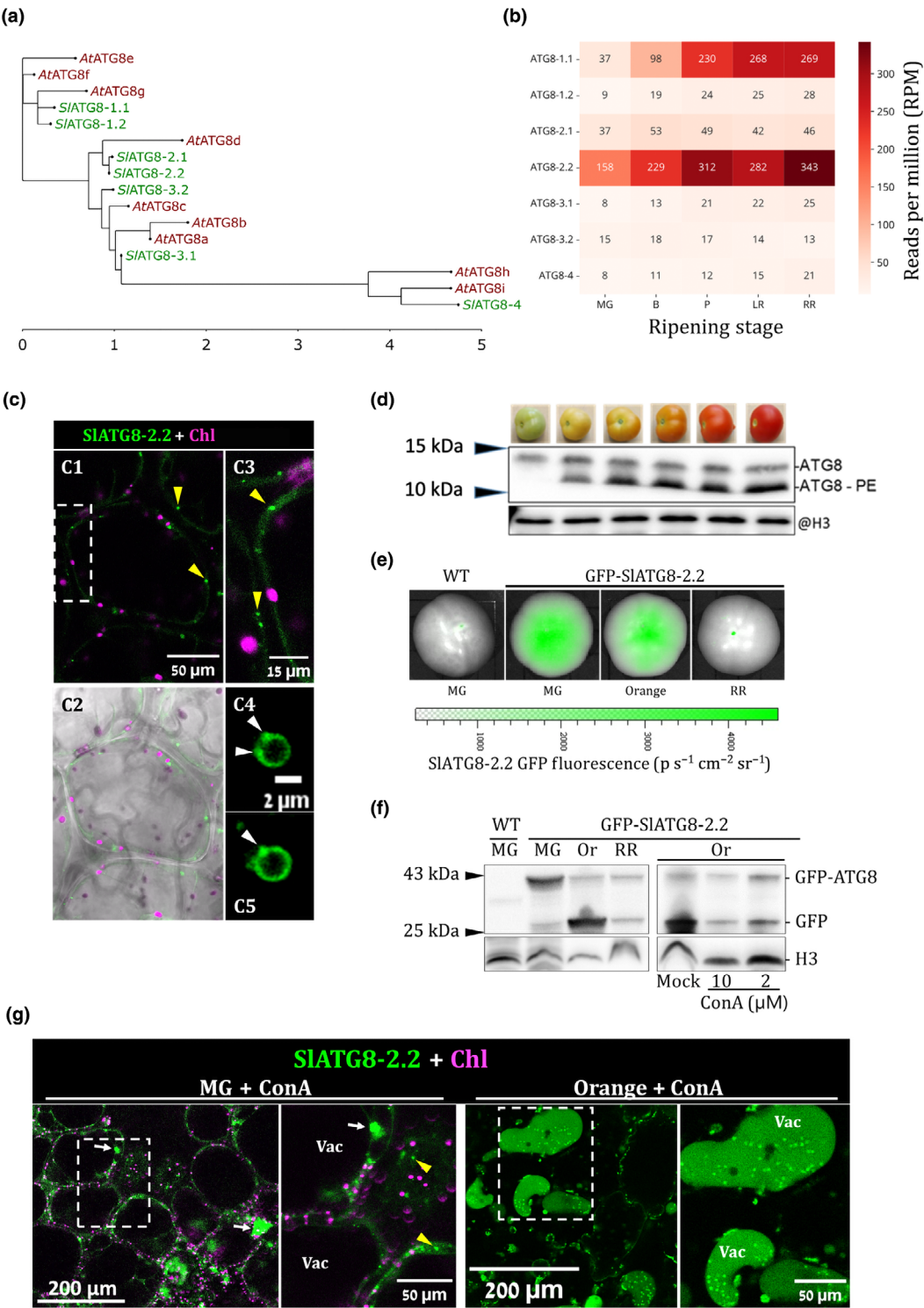


Fig. 1 Autophagy activity climaxes at mid-ripening. (a) A phylogenetic tree showing the four *Solanum lycopersicum* (tomato) ATG8 (SIATG8) family subgroups with the related *Arabidopsis thaliana* AtATG8 members. The scale bar represents branch length in substitutions per site. (b) Modified representation of SIATG8 family members' relative transcript expression in reads per million. Data obtained from SGN-TEA. (c) Confocal laser-scanning microscopy (CLSM) imaging of fruit endocarp cells expressing GFP-SIATG8-2.2 (green). The magenta signal represents Chl autofluorescence. Yellow arrowheads point toward autophagosomes. Image C2 also includes the bright-field channel. Image C3 is an enlargement of the area defined with a dashed rectangle at C1. Images C4 and C5 show a developing autophagosome imaged 1 min apart. White arrowheads in image C4 denote the estimated location of phagophore edges. The white arrowhead in image C5 points toward the estimated autophagosome closure site. (d) Total pericarp proteins from six ripening stages were separated in resolving gel supplemented with 6 M urea and immunoblotted with @ATG8 antibodies (Abcam). Histone 3 (@H3; Millipore) serves as a loading control. A representative blot of three biological repeats is shown. (e) Fluorescence emission from GFP-SIATG8-2.2 fruits at three ripening stages: mature-green (MG), orange, and red-ripe (RR), imaged using *in vivo* imaging system. None of the 22 RR-stage fruits examined exhibited a detectable fluorescence signal. (f) Total pericarp proteins of GFP-SIATG8-2.2 fruits from three ripening stages and wild-type (WT) MG-stage as control were immunoblotted with @GFP. Histone 3 (H3) serves as a loading control. Orange-stage (Or) fruits were also treated with the indicated concentrations of concanamycin A (ConA) or mock (DMSO). Representative blots of three biological repeats are shown. (g) CLSM imaging of ConA-treated endocarp cells of MG- and orange-stage GFP-SIATG8-2.2 fruits. The magenta signal represents Chl autofluorescence. Yellow arrowheads point toward autophagosomes. White arrows denote the location of cytosolic aggregates, potentially culminating due to their inability to degrade. Representative images of 10 replicates (representing > 50 cells) per ripening stage are shown. No autophagic bodies were detected in any of the MG-stage cells. Vac, vacuole lumen.

et al., 2015; Li *et al.*, 2015; Masclaux-Daubresse *et al.*, 2017). Therefore, knockout or constitutive knockdown of any key ATG gene would result in pleiotropic effects, preventing the understanding of ripening-specific roles. To overcome this, we applied two approaches. First, we used VIGS directly in the MG-stage *Del/Ros1* tomato fruits, harboring the Snapdragon transgenes *Delila* (*DEL*) and *Rosea 1* (*ROS1*) driven by the E8 ripening-induced promoter. Therefore, silencing *Del/Ros1*, which prevents the ripening-associated appearance of purple fruits (Orzaez *et al.*, 2009), is a visual indicator for silencing (Fig. 2a; D/R vs NT fruits). Silencing of the core autophagy genes, *SIATG2* or *SIATG7*, each with *DEL/ROS1* (*D/R/ATG2-VIGS* or *D/R/ATG7-VIGS*, respectively), resulted in SIATG8 accumulation, presumably due to its decreased turnover (Fig. S1a). This is consistent with the accumulation of AtATG8 in *Arabidopsis atg2* and *atg7* mutants (Munch *et al.*, 2014; Kang *et al.*, 2018; Luo *et al.*, 2023). Phenotypically, silencing *SIATG2* resulted in accelerated color transition (Fig. 2a). A quantitative examination of fruit populations' green-to-red transition, manifested by declining hue angle values, showed an accelerated color transition of *ATG2*-silenced fruits (*D/R/ATG2-VIGS*) relative to reference fruits (*D/R-VIGS*; Fig. 2b). A similar outcome was revealed following silencing of *SIATG7* (*D/R/ATG7-VIGS*), albeit with differences observed at an earlier time point (Fig. S1b). Moreover, *D/R/ATG2-VIGS* fruits exhibited accelerated fruit softening as indicated by firmness measurements (Fig. 2c).

For the second approach, we targeted *SIATG4*. Similar to most ATG8 members, its expression also increases along ripening progression, suggesting they may be synchronized to allow proper lipidation or delipidation of ATG8 proteins (Fig. S2). For ripening-specific silencing, we generated transgenic lines harboring a previously confirmed *ATG4-RNAi* construct (Alseekh *et al.*, 2022), albeit under the regulation of a ripening-induced promoter (*E8::SIATG4-RNAi*). We focused on line no. 18 (L18), which exhibited significant silencing, and L9, which was revealed as a relatively weak line (Fig. 2d). Since ATG4 may act in both lipidation and delipidation of ATG8 (Zou *et al.*, 2025), we reasoned that autophagy activity assessment via ATG8-PE levels would not fit here. Therefore, we turned to examine the levels of

neighbor of BRCA 1 (*NBR1*), a selective-autophagy cargo receptor known to accumulate under autophagy deficiency (Fig. S3a) and to reflect the autophagy flux status (Bassham, 2015; Yoshii & Mizushima, 2017; Zhao *et al.*, 2022). There are two predicted *NBR1* genes in tomatoes: *SINBR1a* and *SINBR1b* (Zhou *et al.*, 2014). Constitutive *ATG4* silencing (in 35S::*ATG4-RNAi* plants (Alseekh *et al.*, 2022)) resulted in the marked accumulation of *SINBR1a* (Fig. S3b).

Consistently, *SINBR1a* accumulated in the *E8::ATG4-RNAi* L18 pink-stage fruits relative to WT pink-stage fruits (Fig. 2e), without a concomitant increase in *SINBR1a* nor in *SINBR1b* transcript levels (Fig. 2f), demonstrating a reduced autophagic breakdown in L18 fruits. Fruits from WT and the transgenic lines were harvested at the MG stage and monitored postharvest for color transition (Fig. 2g). On average, L18 fruits initiated earlier ripening and reached full ripeness 7 d before WT and L9 fruits (Fig. 2h). Notably, accelerated ripening was also observed in nondetached fruits of *E8::SIATG4-RNAi* lines L15 and L18 (Fig. S4). Altogether, these results demonstrate that autophagy is involved in ripening restriction.

Previously, constitutive silencing of *SIATG4* (35S::*ATG4-RNAi*) was reported to result in early tomato leaf senescence (Alseekh *et al.*, 2022), a canonical phenotype of autophagy deficiency, which has the potential to affect fruit development and ripening. To verify that our ripening-context (*E8::ATG4-RNAi*) lines phenotype is restricted to fruits, we visually monitored leaves from L9, L15, and L18, as well as their electrolyte leakage measurements. These tests showed no significant differences in leaf senescence of the silencing lines relative to WT leaves (Fig. S5a–c). To assess the tissue-dependent activity of the E8 promoter, we quantified the expression of the cloned *ATG4* fragment (Fig. S5d) in pink-stage fruits and leaves of WT and L18 plants. This showed that its expression in L18 fruits is, on average, almost 10 times that of the expression in WT fruits (the latter representing the expression of the native WT *ATG4* gene). On the contrary, there were no significant differences in *ATG4* expression in the leaves of these genotypes (Fig. S5e). These data suggest that E8 promoter activity, driving *ATG4* silencing, is indeed restricted to fruits.

To examine whether the impact of autophagy on ripening is linked to ethylene, we treated WT, L18, and L9 fruits with the ethylene antagonist, 1-MCP, before hue measurements were taken

to assess color transition. Fruits were harvested at a relatively advanced color stage (hue value of ≈ 105) to minimize the ripening initiation gap. 1-Methylcyclopropene abolished the ripening

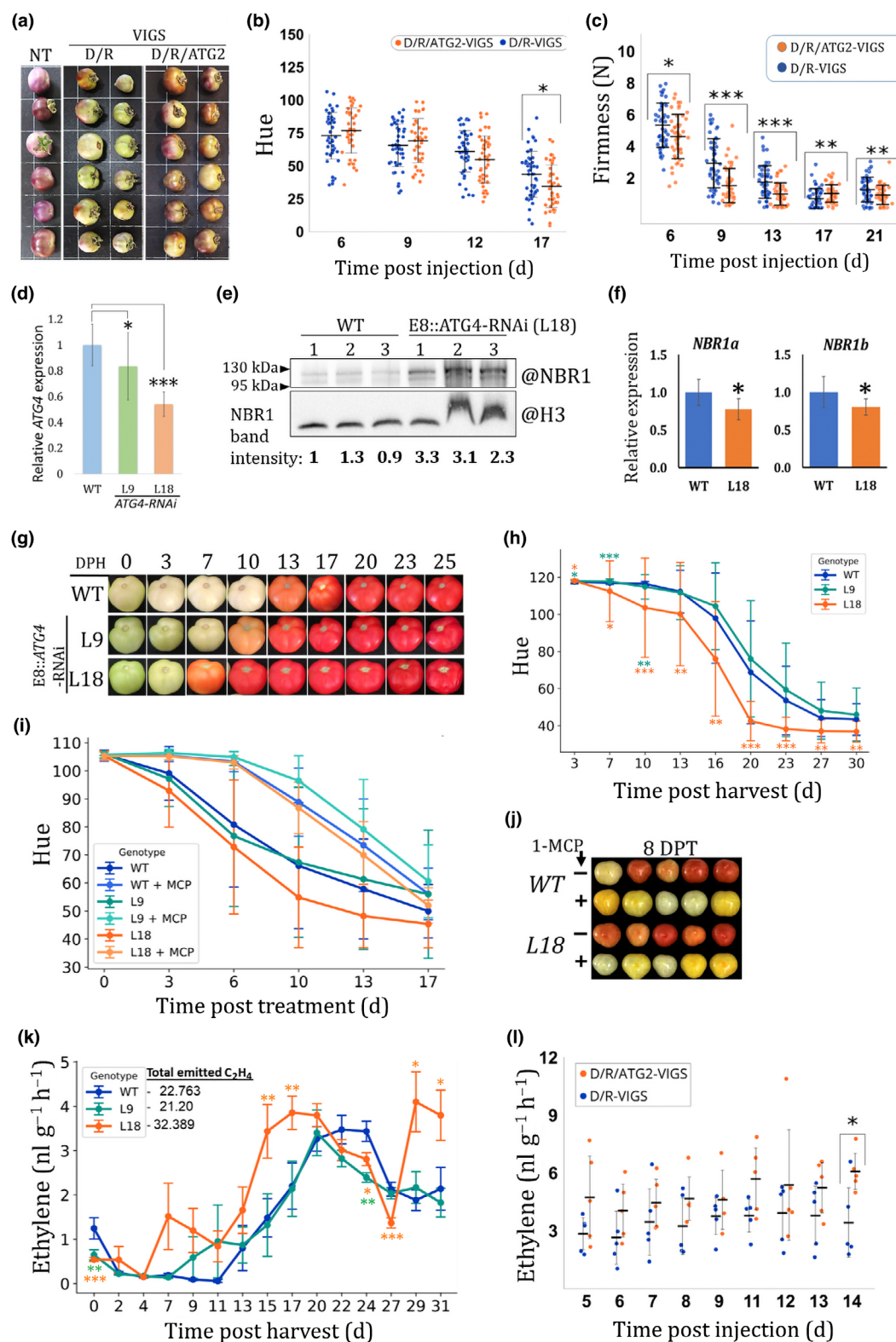


Fig. 2 Silencing *SIATG2* or *SIATG4* in mature fruits results in accelerated ripening and ethylene production. (a–c) D/R-VIGS, silencing of *Del/Ros1*. D/R/ATG2-VIGS, silencing of *Del/Ros1* and *ATG2*. D/R/ATG7-VIGS, silencing of *Del/Ros1* and *ATG7*. (a) Representative *Del/Ros1* tomato fruits at 10 d post injection of *Agrobacterium tumefaciens* (*Agrobacterium*) strain GV3101 cells harboring the indicated virus-induced gene silencing (VIGS) constructs. NT, nontreated. (b) Quantification of the green-to-red color transition (hue) of VIGS-treated fruits at the indicated days post *Agrobacterium* injection. Decreasing hue values indicate color transition. Values are the mean \pm SD ($n = 30$; each value represents the average of three technical measurements for each fruit). (c) Firmness measurements of populations of VIGS-treated fruits. Firmness is displayed as the force in Newton (N) required to achieve a similar probe penetration (see the [Materials and Methods](#) section) on different days post *Agrobacterium* injection. Values are the mean \pm SD ($n > 30$). (d) Relative expression of *SIATG4* in pink-stage fruits from the wild-type (WT) and two E8::ATG4-RNAi lines was measured by quantitative reverse transcription polymerase chain reaction (RT-PCR). Values are the mean \pm SD after normalization to three reference genes (*TIP4*, *Actin*, and *GAPDH*). Significance was tested relative to WT using one-tailed and paired Student's *t*-test $n = 9$. *, $0.01 < P < 0.05$; ***, $P < 0.001$. (e) Total pericarp proteins of pink-stage fruits from the WT and E8::ATG4-RNAi line L18 were immunoblotted with @NBR1 antibodies. For each genotype, three biological replicates are presented (noted as 1–3). Histone 3 (@H3; Millipore) serves as a loading control. Neighbor of BRCA 1 band intensities (quantified using *IMAGEJ*) were normalized to the H3 loading control bands and are presented as the ratio relative to the far-left band (WT1). (f) Relative expression of *SINBR1a* (*Solyc03g112230*) and *SINBR1b* (*Solyc06g071770*) in the pericarp of pink-stage fruits from WT and L18 was measured by quantitative RT-PCR. Values are the mean \pm SD after normalization relative to two reference genes (*Actin* and *GAPDH*) with similar results. Three biological (each representing three fruits) and technical replicates were performed. Significance was tested relative to the WT using one-tailed and paired Student's *t*-tests. *, $P < 0.01$. (g) WT, L9, and L18 tomato fruits across 25 d post harvest. The first fruit to initiate ripening out of the sampled population of each genotype is shown here. (h) Quantification of the green-to-red color transition (hue) of WT, L9, and L18 fruits at the indicated days post harvest. Values are the mean \pm SD ($n = 30$). (i) Quantification of green-to-red color transition (hue) of WT, L9, and L18 fruits, treated or not with 1-methylcyclopropane. Values at the indicated days post treatment are the mean \pm SD ($n = 10$). (j) Representative WT and L18 fruits from the experiment described in (i). (k) Ethylene production in WT, L9, and L18 tomato fruits over 31 d post harvest. The numbers next to the key represent total ethylene production, on average, for each genotype during the entire measurement duration. Values are mean \pm SE ($n = 30$; each measurement represents an average of three fruits). (l) Ethylene production from *Del/ROS1* fruits following *Del/Ros1* VIGS-mediated silencing (D/R-VIGS as control) or fruits additionally silenced in *ATG2* (D/R/ATG2-VIGS). Values at the indicated days post injection of *Agrobacterium* cells are the mean \pm SD ($n = 5$; each measurement recorded from three pooled fruits). Significance was tested relative to controls (D/R-VIGS in (b, c, l), or WT in (h, k)) for each time point. Either unpaired and two-tailed Student's *t*-tests or the *Mann–Whitney U* test was performed based on population distribution and variance (see the [Materials and Methods](#) section). No asterisk, not significant; *, $0.01 < P < 0.05$; **, $0.001 < P < 0.01$; ***, $P < 0.001$.

advantage of L18, which exhibited similar delayed ripening dynamics as the WT fruits (Fig. 2i,j), suggesting that autophagy might regulate ripening via interaction with ethylene. Examination of ethylene emission showed earlier climacteric phase onset and higher ethylene production in L18 than in WT and L9 fruits. On average, L18 initiated ethylene production 7 d before WT and 3 d before L9 fruits. However, differences at 7–13 d post harvest were found to be statistically insignificant (using the *Mann–Whitney U* test) due to the high variance usually found within fruit populations around the ripening initiation time. Notably, L18 fruits reached ethylene production climax 5 d before WT and 3 d before L9 (Fig. 2k). Moreover, pink-stage L18 fruits did not show significant alteration in the expression of tomato *ACC-Oxidase 1*, *ACC-Oxidase 4*, *ACC-Synthase 2*, *ACC-Synthase 4*, *Polygalacturonase*, or *Expansin 1* relative to their levels in WT pink-stage fruits (Fig. S6). These genes are involved in climacteric ethylene production and fruit softening (Li *et al.*, 2021), suggesting that autophagy's regulation of ripening is not at the level of transcription. We further examined ethylene emission from the *Del/Ros1/ATG2*-VIGS fruits compared with the *Del/Ros1*-VIGS reference. Experiments showed elevated ethylene production in the *ATG2*-silenced fruits throughout the experiment, albeit significantly higher at 14 d post injection (Fig. 2l). A similar experiment testing *ATG7*-VIGS revealed a similar outcome, with a significantly elevated ethylene emission at 7- and 8 d post injection (Fig. S1c). These results, together with the 1-MCP treatment data, suggest autophagy affects ripening via its impact on ethylene production. That said, we currently cannot exclude the possible involvement of additional hormones known to interact with ethylene and to affect ripening, such as abscisic acid and auxin (Fenn & Giovannoni, 2021).

To gain further insight into the autophagy-ripening and autophagy-ethylene crosstalk, we examined its activity in fruits of the ripening mutants, *never-ripe* (*nr*) and *colorless nonripening* (*cnr*). *NR* encodes an ethylene receptor (Tieman *et al.*, 2000), while *CNR* encodes a SQUAMOSA promoter-binding protein-like transcription factor (Wang *et al.*, 2020). In WT, *SINBR1a* was detected at the MG and turning stages (40 and 47 d post anthesis (DPA), respectively) and significantly reduced at RR (54 DPA), potentially reflecting an increased flux of NBR1 toward the end of the ripening process. Notably, *SINBR1a* levels were significantly higher in *nr* than in WT fruits at all three stages examined. On the contrary, *SINBR1a* was undetectable at any of the *cnr* fruits examined (Fig. S7a). Quantitative PCR showed no significant difference in *SINBR1a* transcript in *nr* relative to WT fruits, suggesting a decreased autophagy activity in *nr* fruits (Fig. S7b). However, we estimate that the *c.* 20% reduction in *NBR1a* expression in *cnr* fruits (Fig. S7b) does not fully explain the lack of *SINBR1* protein detection, suggesting strong autophagy flux in *cnr* fruits. Although we currently cannot provide a clear explanation, we do note that *cnr*, which is impaired in ethylene production, appears to show hyperautophagic activity, whereas *nr*, which is impaired downstream of ethylene production, shows the opposite. In other words, the negative correlation between ethylene production and autophagy activity is yet again apparent in these fruit-ripening mutants.

To see whether autophagy impacts ethylene beyond ripening, we examined *Arabidopsis atg2-1* knockout seedlings under the triple-response assay, a known test for detecting ethylene-sensitive or ethylene-insensitive mutants (Merchante & Stepanova, 2017). Overall, the *atg2* mutants did not show altered root growth relative

to *Col-0* seedlings in the dark. However, differences were significant following ACC application (Fig. 3a,b). A similar examination of *atg5-1* and *atg7-2* autophagy-deficient mutants and *ebf2-3* as a

known ethylene hypersensitive mutant (Potuschak *et al.*, 2003) revealed a similar outcome, except for *atg5* seedlings exhibiting a shorter root already under dark treatment (Fig. S8a,b). Notably,

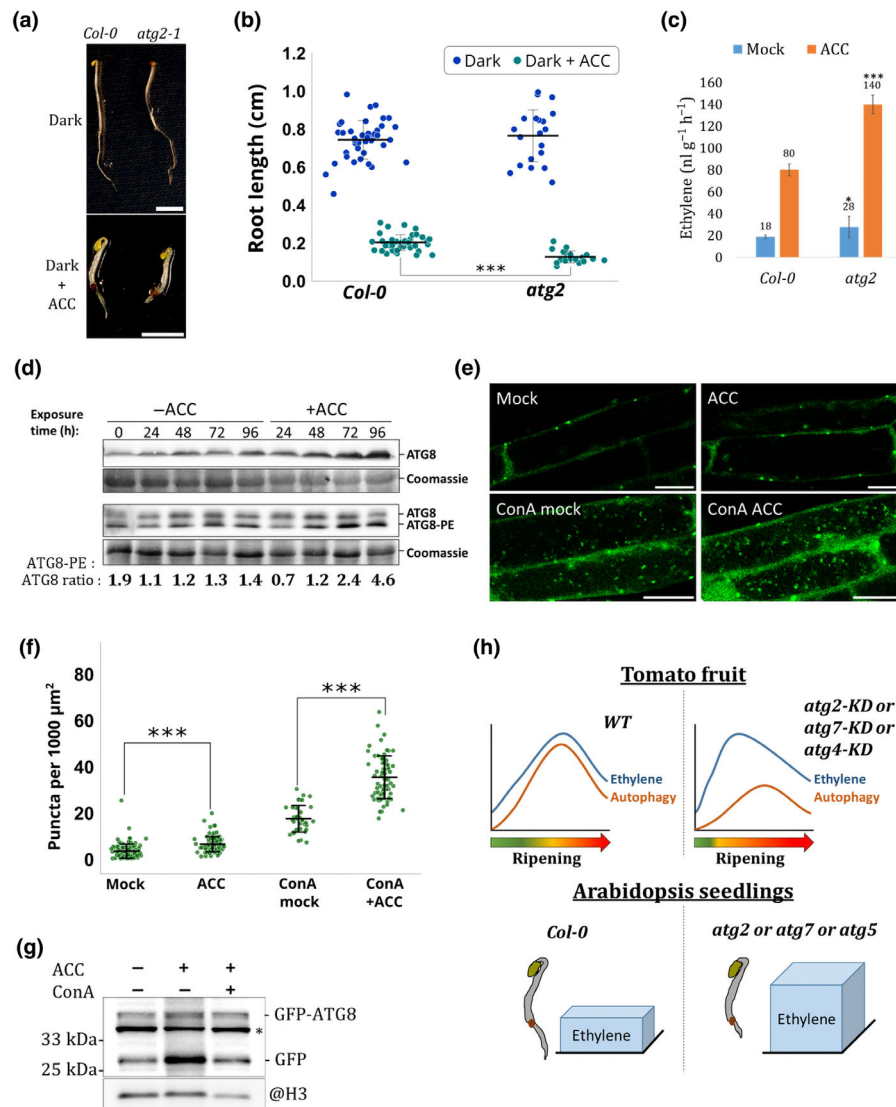


Fig. 3 Autophagy-deficient *atg2* *Arabidopsis* seedlings display increased ethylene emission and 1-aminocyclopropane-1-carboxylate (ACC) induces autophagy, and the current working model. (a) Representative *Arabidopsis* seedlings of the indicated genotypes were assessed for ACC-induced triple-response assay (dark-grown, etiolated seedlings, with or without ACC treatment; see the [Materials and Methods](#) section). Bars, 0.25 cm. (b) Root length measurements of seedlings subjected to the triple-response assay. Values represent means \pm SD ($n > 19$). (c) Ethylene production from 10-d-old *Arabidopsis* seedlings. Values represent mean \pm SD ($n = 5$, each measurement recorded from 30 pooled seedlings). (d) Total protein extracts of *Arabidopsis* seedlings, grown with or without ACC-containing medium for the indicated time points (in hours), were immunoblotted with @ATG8. The upper lane shows standard separation, while the lower lane shows separation in a 6 M urea-supplemented gel. Coomassie staining serves as loading control. (e) Representative confocal images of *Arabidopsis* root cells expressing GFP-ATG8e following treatment with ACC, mock, concanamycin A (ConA) + mock, or ConA + ACC. Bars, 20 μ m. (f) Quantification of GFP-ATG8e puncta in image slices of plants treated as described in (e). Numbers were normalized to image area (1000 μ m²). $n > 35$. (g) Total proteins of transgenic GFP-ATG8e *Arabidopsis* seedling roots that were treated with mock, ACC (20 μ M), or ACC and ConA (1 μ M) for 72 h before immunoblotting with @GFP. The asterisk denotes a nonspecific protein band, as can be seen in *Col-0* samples (Supporting Information Fig. S9a). Histone 3 (H3) serves as a loading control. Representative blots of two biological repeats are shown. (h) Representation of ethylene and autophagy dynamics along wild-type (WT) or ATG knockdown (KD) fruit ripening. In WT, autophagy and ethylene share similar dynamics, and autophagy participates in buffering ethylene levels. In ATG KD (*atg2-KD*, *atg7-KD*, or *atg4-KD*) fruits, the milder buildup of autophagy results in earlier induction of climacteric ethylene production and, hence, earlier ripening. Below is a representation of ethylene production in *Col-0* or ATG-deficient *Arabidopsis* seedlings and its impact on root elongation. Following ACC application, *atg5*, *atg2*, or *atg7* mutants produce more ethylene, which may lead to their reduced root length under the 'triple-response' assay conditions (ACC + darkness) compared with *Col-0*. Significance was tested relative to controls (*Col-0* in (b, c) or mock (f)). Either unpaired and two-tailed Student's *t*-tests or the Mann–Whitney *U* test was performed based on population distribution and variance (see the [Materials and Methods](#) section). No asterisk, not significant; *, 0.01 $< P < 0.05$; **, 0.001 $< P < 0.01$; ***, $P < 0.001$.

atg2, *atg5*, and *atg7* seedlings exhibited between 1.75- and threefold increase in ethylene emission relative to *Col-0* following ACC treatment, while *atg2* and *atg7* produced significantly more ethylene even under mock treatment (Figs 3c, S8c). These results suggest that the root phenotype of *atg* mutants following ACC application may be due to increased ethylene production, highlighting a potentially general role for autophagy in ethylene repression.

ACC induces autophagy activity

It was previously reported that ACC induces autophagy based on GFP-ATG8a foci numbers (without ConA), GFP-release assay, and expression of the selective-autophagy cargo receptor, NBR1 (Rodríguez *et al.*, 2020). Considering our observations, we wanted to reaffirm this with complementary approaches. First, we tested ATG8 levels in *Arabidopsis Col-0* seedlings subjected to ACC or mock. Results showed that both total ATG8 (Fig. 3d, upper blot) and ATG8-PE (Fig. 3d, lower blot) levels were higher in ACC-treated seedlings at 72 and 96 h post treatment. Then, we followed GFP-ATG8e in *Arabidopsis* roots subjected to combinations of ACC, ConA, or mock (Fig. 3e). Quantification revealed an increased number of puncta whether ACC was applied solely or combined with ConA, demonstrating that ACC increases autophagosomes production and their flux to the vacuole (Fig. 3f). Examination of GFP-ATG8e using the GFP-release assay supported the microscopy results, showing increased flux following 72 h of ACC treatment, which was reduced with the addition of ConA (Fig. 3g). To examine whether ACC reflects ethylene's function rather than ACC-specific function, we further assessed GFP-ATG8e flux following ethylene application. Ethylene (2 ppm) induced autophagy flux, yet at an earlier time point (48 h) than 20 μ M ACC and quite transiently (Fig. S9a). We speculated that the time difference in reaching autophagy flux between ACC and ethylene might be related to the concentrations applied. Indeed, when 2 μ M ACC was applied (instead of the 20 μ M in Fig. 3g), an earlier flux at 48 h was apparent (Fig. S9b). Together with the report by Rodríguez *et al.* (2020), these results confirm the ability of ACC and ethylene to induce autophagy.

Discussion

It is well-accepted that there is a physiological and molecular resemblance between ripening and senescence, as seen in dry fruits such as *Arabidopsis* siliques (Seymour *et al.*, 2013; Gómez *et al.*, 2014). Indeed, large-scale data analysis suggested that three types of transcriptional circuits controlling ethylene-dependent ripening have evolved from senescence or floral organ identity pathways (Lü *et al.*, 2018). Autophagy is an antisenescence and antiaging mechanism in plants and animals (Liu & Bassham, 2012; Minina *et al.*, 2018; Aman *et al.*, 2021), reconciling with a repressive effect on ripening. We propose that the milder buildup of autophagic capacity in the *SLATG*-silenced fruits permits earlier and elevated ethylene production, leading to accelerated ripening (Fig. 3h, upper panel). Intriguingly, the participation of autophagy

in nonclimacteric fruit ripening of pepper and strawberry was recently reported (López-Vidal *et al.*, 2020; Sánchez-Sevilla *et al.*, 2021). Contrary to our results, it was concluded that autophagy acts in strawberry ripening promotion. If so, we cannot rule out the possibility of autophagy having contradicting roles in climacteric and nonclimacteric fruits. An intriguing possibility is that this reflects the different impacts of ethylene on both fruit types (Perotti *et al.*, 2023). The increased sensitivity of *Arabidopsis atg5*, *atg2*, and *atg7* to ACC, coupled with their elevated ethylene production (Figs 3a–c, S8), suggests that the repressive effect of autophagy is potentially widespread and may extend to other roles of ethylene beyond ripening, for example during root elongation (Fig. 3h, lower panel). However, we note that fruit ripening and root elongation are independent processes in which identical molecular mechanisms are not necessarily expected to exhibit similar functions. Therefore, the fact that autophagy restricts both of them does not suggest they are linked but rather the outcome of the repressive impact of autophagy on ethylene in both systems. Although the transcript level of genes involved in ethylene production was reportedly elevated in *atg5* and *atg9 Arabidopsis* mutants (Masclaux-Daubresse *et al.*, 2014), we have not detected a similar trend in our *ATG4*-RNAi L18 fruits (Fig. S6), potentially highlighting the different manner of regulation between both systems.

As it might be difficult to interpret the buildup of autophagy as a repressive mechanism while ripening is ongoing, we wish to clarify this point. Let us assume that ripening progression is determined by the sum of mechanisms that promote and repress it, with the pace determined by their cumulative effects. In other words, such a highly regulated process would require functional breaks from its initiation to control process onset and their full performance at full speed (in our case, at the turning stage) in order to prevent loss of control (i.e. to mediate the transition from climacteric to postclimacteric ethylene production). In a similar manner, autophagy activity increases with leaf senescence progression, although it delays senescence, as is clearly seen in various *atg* mutants (Yoshimoto *et al.*, 2009). That said, it is not yet fully understood how ripening is initiated. Changes to histone marks and DNA methylation seem to be necessary and are associated with ripening gene activation (Lü *et al.*, 2018; Li *et al.*, 2021). Here, we propose autophagy as an additional layer of regulation.

Several questions emerge from this study. First, how does autophagy limit ethylene? This may happen via the selective degradation of ethylene or ACC production components, such as ACC-Synthase or ACC-Oxidase enzymes (Houben & Van de Poel, 2019; Park *et al.*, 2021). Elimination of even further upstream precursors or other regulatory elements of ethylene production is another possibility. Finally, it cannot be excluded that autophagy may also regulate ethylene signaling components (Binder, 2020). Notably, the ability of ACC to induce autophagy highlights a potential feedback loop for ethylene regulation. Unlike ethylene, ACC levels were reported to continuously increase along with ripening (Van de Poel *et al.*, 2012). Additional questions are as follows what is the weight of ethylene in the well-known early senescence phenotype of autophagy mutants? Especially since, so far, it has mostly been associated

with salicylic acid (Yoshimoto *et al.*, 2009). Finally, does autophagy regulate ripening solely via its impact on ethylene? Although the autophagy-ethylene crosstalk seems significant for ripening progression, it is reasonable to assume that several components, such as protein complexes and organelles, not necessarily related to ethylene, would be recycled via selective-autophagy during ripening (Clavel & Dagdas, 2021; Eckardt *et al.*, 2024). Further studies are required to settle these questions.

Acknowledgements

This research was supported by research grant no. IS-5553-22 from BARD, The United States–Israel Binational Agricultural Research and Development Fund, the Israeli Ministry of Agriculture and Rural Development research grant 20-06-0018, and the Israel Science Foundation (ISF) grant no. 1897/23 to S. Michaeli and Emmy Noether Fellowship GZ: UE188/2-1 from the Deutsche Forschungsgemeinschaft to SÜ. We thank Dr Tamar Avin-Wittenberg (Hebrew University) for providing the 35S::ATG4-RNAi plasmid, Dr Yasin Dagdas (Gregor Mendel Institute, Vienna) for sharing the 35S::GFP-StATG8-2.2 plasmid, Prof. Asaph Aharoni (Weizmann Institute) for providing the Del/Ros1 tomato seeds and the virus-induced gene silencing (VIGS)-related pRTV2 vector, Dr Yana Kazachkova for her assistance in establishing the fruit VIGS system in our laboratory, Prof. Elazar Fallik (Volcani Institute) for providing tomato fruits for some of our initial experiments, and Dr Alexander (Sasha) Goldshmidt (Volcani Institute) for sharing with us *never-ripe*, *colorless nonripening*, and wild-type (Ailsa Craig) tomato fruits. We also appreciate the scientific discussions held with all who are mentioned here and the helpful comment of Prof. Jim Giovannoni (Boyce Thompson Institute, USA) during a scientific meeting.

Competing interests

None declared.


Author contributions

GK, PKP, EQ, S Mursalimov, JD, SA-T, EL and S Michaeli designed experiments and conducted experiments. GK performed all virus-induced gene silencing-related experiments, data and statistical analysis, phylogenetic tree construction and autophagy activity assays in tomatoes. PKP generated the E8:ATG4-RNAi tomato lines and performed most *Arabidopsis* experiments and SINBR1 immunoblots. EQ assisted in several aspects of the study and conducted hue, firmness, ethylene measurements and tomato fruit GFP-release assay blots. S Mursalimov performed confocal microscopy and quantification in *Arabidopsis*. JD examined the E8:ATG4-RNAi lines and performed qPCRs. SA-T assisted in hue, firmness, and ethylene measurements and performed the 1-MCP experiments. EL performed qPCR. JXL and KS generated the GFP-ATG8-2.2 tomato lines. SÜ supervised students and contributed to the draft. All authors discussed the results and contributed to editing the manuscript. S Michaeli conceived

the study, supervised the work, and wrote the manuscript. GK and PKP contributed equally to this work.

ORCID


Jyoti Devi  <https://orcid.org/0000-0002-8493-7102>

Girishkumar Kumaran  <https://orcid.org/0000-0003-3000-7978>

Jia Xuan Leong  <https://orcid.org/0000-0001-6016-1445>

Elena Levin  <https://orcid.org/0000-0001-6398-9651>


Simon Michaeli  <https://orcid.org/0000-0003-0123-6544>

Sergey Mursalimov  <https://orcid.org/0000-0001-6935-4331>

Pradeep Kumar Pathak  <https://orcid.org/0009-0008-3976-301X>










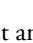
Ebenezer Quandoh  <https://orcid.org/0000-0002-6923-7714>

Kyrylo Schenstnyi  <https://orcid.org/0000-0003-1595-6382>

Suayib Üstün  <https://orcid.org/0000-0002-8049-296X>

Data availability

Accession nos. associated with this work: Solyc01g108160 (ATG2), Solyc11g068930 (ATG7), Solyc01g006230 (ATG4), Solyc08g078820 (SIATG8-1.1), Solyc07g064680 (SIATG8-2.2), Solyc03g112230 (SINBR1a), and Solyc06g071770 (SINBR1b). All research data are contained in the article (Figs 1–3) and the Supporting Information (Figs S1–S9; Table S1; Videos S1, S2).

Girishkumar Kumaran^{1*} , Pradeep Kumar Pathak^{1*} , Ebenezer Quandoh^{1,2} , Jyoti Devi¹ , Sergey Mursalimov¹ , Sharon Alkalai-Tuvia¹, Jia Xuan Leong³ , Kyrylo Schenstnyi³ , Elena Levin¹ , Suayib Üstün³  and Simon Michaeli^{1*} 

¹Department of Postharvest Sciences, Institute of Postharvest and Food Sciences, Agricultural Research Organization (ARO), Volcani Institute, Rishon-LeZion, 7505101, Israel;

²The Robert H. Smith Faculty of Agriculture, Food and Environment, Hebrew University of Jerusalem, Rehovot, 7610001, Israel;

³ZMBP – General Genetics, University of Tübingen, Auf der Morgenstelle 32, 72076, Tübingen, Germany

(*Author for correspondence: email simonm@volcani.agri.gov.il)

[†]These authors contributed equally to this work.

References

- Alseekh S, Zhu F, Vallarino JG, Sokolowska EM, Yoshida T, Bergmann S, Wendenburg R, Bolze A, Skirycz A, Avin-Wittenberg T *et al.* 2022. Autophagy modulates the metabolism and growth of tomato fruit during development. *Horticulture Research* 9: uhac129.
- Aman Y, Schmauck-Medina T, Hansen M, Morimoto RI, Simon AK, Bjedov I, Palikaras K, Simonsen A, Johansen T, Tavernarakis N *et al.* 2021. Autophagy in healthy aging and disease. *Nature Aging* 1: 634–650.
- Avin-Wittenberg T, Bajdzienko K, Wittenberg G, Alseekh S, Tohge T, Bock R, Gialalisco P, Fernie AR. 2015. Global analysis of the role of autophagy in cellular metabolism and energy homeostasis in *Arabidopsis* seedlings under carbon starvation. *Plant Cell* 27: 306–322.

- Bassham DC. 2015. Methods for analysis of autophagy in plants. *Methods* 75: 181–188.
- Batu A. 2004. Determination of acceptable firmness and colour values of tomatoes. *Journal of Food Engineering* 61: 471–475.
- Binder BM. 2020. Ethylene signaling in plants. *Journal of Biological Chemistry* 295: 7710–7725.
- Clavel M, Dagdas Y. 2021. Proteasome and selective autophagy: brothers-in-arms for organelle quality control. *Current Opinion in Plant Biology* 63: 102106.
- Del Chiaro A, Grujic N, Zhao J, Papareddy RK, Gao P, Ma J, Loeffke C, Bhattacharya A, Gruetzner R, Bourguet P *et al.* 2024. Nonuple atg8 mutant provides genetic evidence for functional specialization of ATG8 isoforms in *Arabidopsis thaliana*. *bioRxiv*. doi: 10.1101/2024.12.10.627464.
- Ding X, Zhang X, Otegui MS. 2018. Plant autophagy: new flavors on the menu. *Current Opinion in Plant Biology* 46: 113–121.
- Eckardt NA, Avin-Wittenberg T, Bassham DC, Chen P, Chen Q, Fang J, Genschik P, Ghafari AS, Guercio AM, Gibbs DJ *et al.* 2024. The lowdown on breakdown: open questions in plant proteolysis. *Plant Cell* 36: 2931–2975.
- Fenn MA, Giovannoni JJ. 2021. Phytohormones in fruit development and maturation. *The Plant Journal* 105: 446–458.
- Giovannoni J, Nguyen C, Ampofo B, Zhong S, Fei Z. 2017. The epigenome and transcriptional dynamics of fruit ripening. *Annual Review of Plant Biology* 68: 61–84.
- Gómez MD, Vera-Sirera F, Pérez-Amador MA. 2014. Molecular programme of senescence in dry and fleshy fruits. *Journal of Experimental Botany* 65: 4515–4526.
- Houben B, Van de Poel B. 2019. 1-Aminocyclopropane-1-carboxylic acid oxidase (ACO): the enzyme that makes the plant hormone ethylene. *Frontiers in Plant Science* 10: 695.
- Huang W, Hu N, Xiao Z, Qiu Y, Yang Y, Yang J, Mao X, Wang Y, Li Z, Guo H. 2022. A molecular framework of ethylene-mediated fruit growth and ripening processes in tomato. *Plant Cell* 34: koac146.
- Jia W, Liu G, Zhang P, Li H, Peng Z, Wang Y, Jemric T, Fu D. 2023. The ubiquitin–26S proteasome pathway and its role in the ripening of fleshy fruits. *International Journal of Molecular Sciences* 24: 2750.
- Kang S, Shin KD, Kim JH, Chung T. 2018. Autophagy-related (ATG) 11, ATG9 and the phosphatidylinositol 3-kinase control ATG2-mediated formation of autophagosomes in Arabidopsis. *Plant Cell Reports* 37: 653–664.
- Kellner R, De la Concepcion JC, Maqbool A, Kamoun S, Dagdas YF. 2017. ATG8 expansion: a driver of selective autophagy diversification? *Trends in Plant Science* 22: 204–214.
- Li F, Chung T, Pennington JG, Federico ML, Kaeppler HF, Kaeppler SM, Otegui MS, Vierstra RD. 2015. Autophagic recycling plays a central role in maize nitrogen remobilization. *Plant Cell* 27: 1389–1408.
- Li S, Chen K, Grierson D. 2021. Molecular and hormonal mechanisms regulating fleshy fruit ripening. *Cells* 10: 1136.
- Liao C-Y, Wang P, Yin Y, Bassham DC. 2022. Interactions between autophagy and phytohormone signaling pathways in plants. *FEBS Letters* 596: 2198–2214.
- Liu Y, Bassham DC. 2012. Autophagy: pathways for self-eating in plant cells. *Annual Review of Plant Biology* 63: 215–237.
- López-Vidal O, Olmedilla A, Sandalio LM, Sevilla F, Jiménez A. 2020. Is autophagy involved in pepper fruit ripening? *Cells* 9: 106.
- Lü P, Yu S, Zhu N, Chen Y-R, Zhou B, Pan Y, Tzeng D, Fabi JP, Argyris J, Garcia-Mas J *et al.* 2018. Genome encode analyses reveal the basis of convergent evolution of fleshy fruit ripening. *Nature Plants* 4: 784–791.
- Luo M, Law KC, He Y, Chung KK, Po MK, Feng L, Chung KP, Gao C, Zhuang X, Jiang L. 2023. Arabidopsis AUTOPHAGY-RELATED2 is essential for ATG18a and ATG9 trafficking during autophagosome closure. *Plant Physiology* 193: 304–321.
- Marshall RS, Vierstra RD. 2018. Autophagy: the master of bulk and selective recycling. *Annual Review of Plant Biology* 69: 173–208.
- Masclaux-Daubresse C, Chen Q, Havé M. 2017. Regulation of nutrient recycling via autophagy. *Current Opinion in Plant Biology* 39: 8–17.
- Masclaux-Daubresse C, Clément G, Anne P, Routaboul J-M, Guiboileau A, Soulay F, Shirasu K, Yoshimoto K. 2014. Stitching together the multiple dimensions of autophagy using metabolomics and transcriptomics reveals impacts on metabolism, development, and plant responses to the environment in Arabidopsis. *Plant Cell* 26: 1857–1877.
- Merchante C, Stepanova AN. 2017. The triple response assay and its use to characterize ethylene mutants in Arabidopsis. In: Binder BM, Eric Schaller G, eds. *Methods in molecular biology. Ethylene signaling: methods and protocols*. New York, NY, USA: Springer, 163–209.
- Michaeli S, Clavel M, Lechner E, Viotti C, Wu J, Dubois M, Hacquard T, Derrien B, Izquierdo E, Lecorbeiller M *et al.* 2019. The viral F-box protein P0 induces an ER-derived autophagy degradation pathway for the clearance of membrane-bound AGO1. *Proceedings of the National Academy of Sciences, USA* 116: 22872–22883.
- Minina EA, Moschou PN, Vetukuri RR, Sanchez-Vera V, Cardoso C, Liu Q, Elander PH, Dalman K, Beganovic M, Lindberg Yilmaz J *et al.* 2018. Transcriptional stimulation of rate-limiting components of the autophagic pathway improves plant fitness. *Journal of Experimental Botany* 69: 1415–1432.
- Munch D, Rodriguez E, Bressendorff S, Park OK, Hofius D, Petersen M. 2014. Autophagy deficiency leads to accumulation of ubiquitinated proteins, ER stress, and cell death in Arabidopsis. *Autophagy* 10: 1579–1587.
- Orzaez D, Medina A, Torre S, Fernández-Moreno JP, Rambla JL, Fernández-del-Carmen A, Butelli E, Martin C, Granell A. 2009. A visual reporter system for virus-induced gene silencing in tomato fruit based on anthocyanin accumulation. *Plant Physiology* 150: 1122–1134.
- Park C, Lee HY, Yoon GM. 2021. The regulation of ACC synthase protein turnover: a rapid route for modulating plant development and stress responses. *Current Opinion in Plant Biology* 63: 102046.
- Perotti MF, Posé D, Martín-Pizarro C. 2023. Non-climacteric fruit development and ripening regulation: ‘the phytohormones show’. *Journal of Experimental Botany* 74: erad271.
- Potuschak T, Lechner E, Parmentier Y, Yanagisawa S, Grava S, Koncz C, Genschik P. 2003. EIN3-dependent regulation of plant ethylene hormone signaling by two Arabidopsis F box proteins: EBF1 and EBF2. *Cell* 115: 679–689.
- Qi H, Wang Y, Bao Y, Bassham DC, Chen L, Chen Q-F, Hou S, Hwang I, Huang L, Lai Z *et al.* 2023. Studying plant autophagy: challenges and recommended methodologies. *Advanced Biotechnology* 1: 2.
- Rodriguez E, Chevalier J, Olsen J, Ansøl J, Kapousidou V, Zuo Z, Svenning S, Loeffke C, Koemeda S, Drozdowskyj PS *et al.* 2020. Autophagy mediates temporary reprogramming and dedifferentiation in plant somatic cells. *EMBO Journal* 39: e103315.
- Sánchez-Sevilla JF, Botella MA, Valpuesta V, Sanchez-Vera V. 2021. Autophagy is required for strawberry fruit ripening. *Frontiers in Plant Science* 12: 688481.
- Seo E, Woo J, Park E, Bertolani SJ, Siegel JB, Choi D, Dinesh-Kumar SP. 2016. Comparative analyses of ubiquitin-like ATG8 and cysteine protease ATG4 autophagy genes in the plant lineage and cross-kingdom processing of ATG8 by ATG4. *Autophagy* 12: 2054–2068.
- Seymour GB, Østergaard L, Chapman NH, Knapp S, Martin C. 2013. Fruit development and ripening. *Annual Review of Plant Biology* 64: 219–241.
- Shibuya K, Niki T, Ichimura K. 2013. Pollination induces autophagy in petunia petals via ethylene. *Journal of Experimental Botany* 64: 1111–1120.
- Shinozaki Y, Nicolas P, Fernandez-Pozo N, Ma Q, Evanich DJ, Shi Y, Xu Y, Zheng Y, Snyder SI, Martin LBB *et al.* 2018. High-resolution spatiotemporal transcriptome mapping of tomato fruit development and ripening. *Nature Communications* 9: 364.
- Sun S, Kang X-P, Xing X-J, Xu X-Y, Cheng J, Zheng S-W, Xing G-M. 2015. *Agrobacterium*-mediated transformation of tomato (*Lycopersicon esculentum* L. cv. Hezuo 908) with improved efficiency. *Biotechnology & Biotechnological Equipment* 29: 861–868.
- Szymanski J, Levin Y, Savidor A, Breitel D, Chappell-Maor L, Heinig U, Töpfer N, Aharoni A. 2017. Label-free deep shotgun proteomics reveals protein dynamics during tomato fruit tissues development. *The Plant Journal* 90: 396–417.
- Tieman DM, Taylor MG, Ciardi JA, Klee HJ. 2000. The tomato ethylene receptors NR and LeETR4 are negative regulators of ethylene response and exhibit functional compensation within a multigene family. *Proceedings of the National Academy of Sciences, USA* 97: 5663–5668.
- Van de Poel B, Bulens I, Markoula A, Hertog MLATM, Dreesen R, Wirtz M, Vandoninck S, Oppermann Y, Keulemans J, Hell R *et al.* 2012. Targeted systems biology profiling of tomato fruit reveals coordination of the Yang cycle and a distinct regulation of ethylene biosynthesis during postclimacteric ripening. *Plant Physiology* 160: 1498–1514.

- Wang R, Lammers M, Tikunov Y, Bovy AG, Angenent GC, de Maagd RA. 2020. The rin, nor and Cnr spontaneous mutations inhibit tomato fruit ripening in additive and epistatic manners. *Plant Science* 294: 110436.
- Yoshii SR, Mizushima N. 2017. Monitoring and measuring autophagy. *International Journal of Molecular Sciences* 18: 1865.
- Yoshimoto K, Jikumaru Y, Kamiya Y, Kusano M, Consonni C, Panstruga R, Ohsumi Y, Shirasu K. 2009. Autophagy negatively regulates cell death by controlling NPR1-dependent salicylic acid signaling during senescence and the innate immune response in Arabidopsis. *Plant Cell* 21: 2914–2927.
- Zess EK, Jensen C, Cruz-Mireles N, la Concepcion JCD, Sklenar J, Stephani M, Imre R, Roitinger E, Hughes R, Belhaj K *et al.* 2019. N-terminal β -strand underpins biochemical specialization of an ATG8 isoform. *PLoS Biology* 17: e3000373.
- Zhao J, Bui MT, Ma J, Künzl F, Picchianti L, De La Concepcion JC, Chen Y, Petsangouraki S, Mohseni A, García-Leon M *et al.* 2022. Plant autophagosomes mature into amphisomes prior to their delivery to the central vacuole. *Journal of Cell Biology* 221: e202203139.
- Zhou J, Wang J, Yu J-Q, Chen Z. 2014. Role and regulation of autophagy in heat stress responses of tomato plants. *Frontiers in Plant Science* 5: 174.
- Zhu T, Zou L, Li Y, Yao X, Xu F, Deng X, Zhang D, Lin H. 2018. Mitochondrial alternative oxidase-dependent autophagy involved in ethylene-mediated drought tolerance in *Solanum lycopersicum*. *Plant Biotechnology Journal* 16: 2063–2076.
- Zou Y, Ohlsson JA, Holla S, Sabljic I, Leong JX, Ballhaus F, Krebs M, Schumacher K, Moschou PN, Stael S *et al.* 2025. ATG8 delipidation is not universally critical for autophagy in plants. *Nature Communications* 16: 403.

Supporting Information

Additional Supporting Information may be found online in the Supporting Information section at the end of the article.

Fig. S1 Impact of *ATG2* or *ATG7* virus-induced gene silencing on ATG8 abundance and of the latter on hue angle readings and ethylene production.

Fig. S2 *SLATG4* expression increases along tomato fruit ripening progression.

Fig. S3 Constitutive silencing of *SLATG4* results in NBR1a accumulation.

Fig. S4 E8::*ATG4*-RNAi fruits display earlier ripening when attached to plants.

Fig. S5 Leaves of E8::*ATG4*-RNAi lines do not show early senescence nor altered expression of the *ATG4* fragment used to drive silencing in the fruits.

Fig. S6 *ATG4* silencing does not result in transcript-level alteration of key ripening-related genes involved in ethylene biosynthesis or softening.

Fig. S7 Fruits of *never-ripe* and *colorless nonripening* mutants exhibit markedly altered levels of SINBR1 protein, while *SINBR1* transcript levels are largely not affected.

Fig. S8 Autophagy-deficient *atg5* and *atg7* *Arabidopsis* seedlings display increased ethylene emission and 1-aminocyclopropane-1-carboxylate sensitivity.

Fig. S9 Ethylene induces ATG8e flux.

Table S1 Primers used in this study.

Video S1 GFP-ATG8-2.2 labeled autophagosomes movement within fruit endocarp cells.

Video S2 GFP-ATG8-2.2 labeled autophagic bodies movement within concanamycin A-treated endocarp cell vacuoles of an orange-stage fruit.

Please note: Wiley is not responsible for the content or functionality of any Supporting Information supplied by the authors. Any queries (other than missing material) should be directed to the *New Phytologist* Central Office.

Key words: ACC, ATG8, autophagy, ethylene, fruit, ripening, tomato.

Received, 24 October 2024; accepted, 10 March 2025.

Disclaimer: The New Phytologist Foundation remains neutral with regard to jurisdictional claims in maps and in any institutional affiliations.